

# Optimization of electrically cooled complex HPGe Detector

---

*Contract No. 4500109716*

*GSI Helmholzzentrum für Schwerionenforschung GmbH  
Planckstraße 1  
64291 Darmstadt*

*28. April 2013*

## CONTENTS

1. Experimental verification of the X-Cooler II thermal power	3
1.1. Block-capacity technique	3
1.2. Temperature dependence of the specific heat	4
1.3. Experimental Set-up	7
2. Measurement of the temperature increase in dependence of the applied thermal load	9
3. Measurement of the heat contact resistance	11
4. Examination of the labyrinths geometry in respect of the heat losses	17
5. References	19

The data sheet of the electromechanical cooling engine X-Cooler II produced by MMR and distributed by ORTEC does not provide information about the thermal power limitation. However this value is critical by dimensioning of the detector assembly especially when cost-effective solution has been sought.

The thermal contact resistance strongly depends on the contact type. In general thermal conductance decreases with temperature becoming very low at cryogenic temperatures. For the designed detector assembly there are no data available which might be used to assess the thermal contact resistance. Though in the second progress report it has been revealed that the thermal conductance significantly influence the temperature deviation along the germanium crystal.

In the current progress report the goal is to verify experimentally the thermal power of the cooling engine and to define the thermal conductance of the critical contacts.

In addition the fixing labyrinth design has been examined in order to evaluate the heat losses.

## 1. Experimental verification of the X-Cooler II thermal power

### 1.1. Block-capacity technique

A non-stationary technique has been proposed for the identification of the heat flux being supplied from the cooling engine X-Cooler II.

The temperature behavior of a good thermoconducting material instantaneously affected by heating or cooling may be described by the concept of the “block-capacity” technique [1].

Within that model temperature is sought as time dependent while the temperature inhomogeneity within the body is taken as negligible. Then

$$(1) \quad \rho c V \frac{dT}{dt} = -\alpha A [T(t) - T_c],$$

where  $\rho$  is the density,  $c$  is the specific heat capacity,  $V$  is the volume, and  $T$  is the temperature of the body. The time is denoted by  $t$ ,  $T_c$  stays for the temperature of the cooling engine and  $\alpha$  is the heat-transfer coefficient.

**Comments:** When incompressible materials with constant density are considered isobaric and isochoric specific heats are identical.

In the case studied a reference time can be defined as

$$(2) \quad t_{ref} = \frac{\rho c V}{\alpha A}$$

and is a measure of the time needed the system under consideration to reach the temperature equilibrium.

A decrease of the system heat-transfer resistance  $R_\alpha \sim 1/\alpha \cdot A$  accelerates the process, while an increase of the system heat capacity  $\rho c V$  leads to its deceleration.

The temperature difference between the cooler temperature  $T_c$  and the initial test temperature  $T_0$  is considered as reference temperature value. So that the dimensionless time and the dimensionless temperature respectively have been defined as

$$(3) \quad \tau = \frac{t}{t_{ref}},$$

$$(4) \quad \theta = \frac{T - T_c}{T_0 - T_c}.$$

Under an assumption that the specific heat is temperature independent the equation (1) can be rewrite as

$$(5) \quad \frac{d\theta}{\theta} = -\tau$$

and (s. also [1])

$$(6) \quad \theta = \exp(-\tau) \text{ or}$$

$$(7) \quad T(t) = T_c + (T_0 - T_c) \cdot \exp\left(-\frac{t}{\rho c V / \alpha A}\right)$$

For small time  $t \ll \rho c V / \alpha A$  is approximately valid

$$(8) \quad T(t) = T_c + (T_0 - T_c) \cdot \left(1 - \frac{t}{\rho c V / \alpha A}\right),$$

or in other words in the beginning of the cooling process the temperature decrease is a linear function on time and the line slope is given with

$$(9) \quad \frac{dT}{dt} = -\frac{\alpha \cdot A}{\rho \cdot c \cdot V} \text{ or } \alpha \cdot A = \frac{dT}{dt} \cdot \rho \cdot c \cdot V.$$

Therefore the heat flux being supplied from the cooling engine is given by

$$(10) \quad Q = \alpha \cdot A \cdot \frac{T_1 - T_0}{t_1 - t_0} = \rho \cdot c \cdot V \cdot \frac{T_1 - T_0}{t_1 - t_0},$$

where  $T_1 - T_0$  presents the temperature decrease being reached within the time  $t_1 - t_0$ .

If the specific heat is a temperature dependent function eq. (10) should be used stepwise for rather small time intervals.

## 1.2. Temperature dependence of the specific heat

In a range from room temperature down to cryogenic one the specific heat of technical materials is rather temperature dependent. This behavior is shown in Fig. 1 and Table 1 (reprinted from [2]). Above 100 K the specific heat decreases slowly. But for lower temperatures the decrease is like  $T^3$  for most materials.

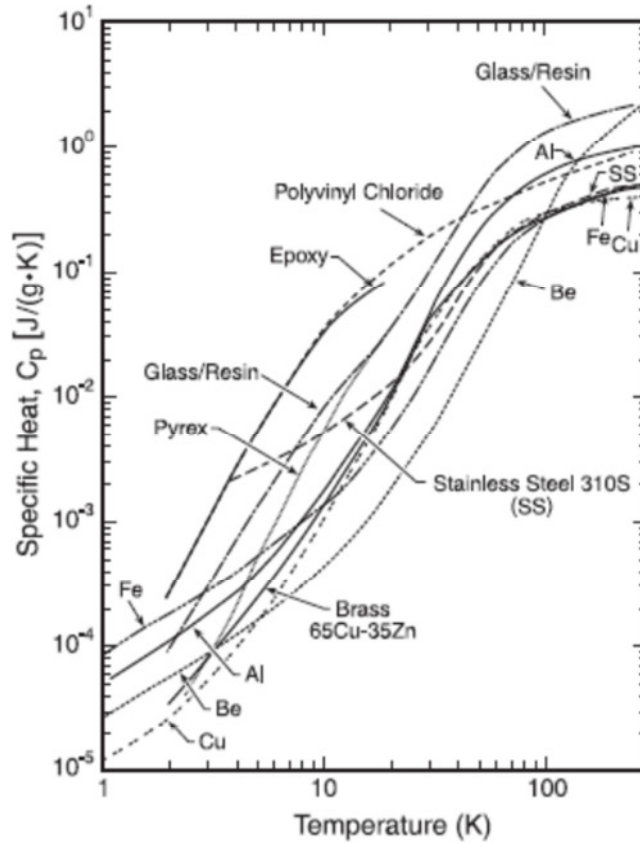


**Fig. 1.** Specific heat for technical materials at cryogenic temperature (from Corruccini and Gniewek 1960, Chang 1977, Touloukian 1966, Johnson, Part II 1960, and White and Meeson 2002). (Reprinted from [2])

Material	77 K [10 <sup>-3</sup> J/kg.K]	100 K [10 <sup>-3</sup> J/kg.K]	150K [10 <sup>-3</sup> J/kg.K]	200 K [10 <sup>-3</sup> J/kg.K]	300 K [10 <sup>-3</sup> J/kg.K]
Metals					
<b>Al</b>	0.336	0.481	0.684	0.797	0.902
<b>Cu</b>	0.192	0.252	0.323	0.356	0.386
Alloys					
<b>Al 2024</b>	0.478	0.354	0.639	0.736	0.855
<b>Al-6061-T6</b>	0.348	0.492	0.713	0.835	0.954

**Table. 1.** Specific heat vs. temperature of technical materials.

Cryogenic team at NIST [8] have critically studied thermodynamical properties of some technical materials and suggested a following formula

$$(11) \quad c = 10^{a+b(\log T)+c(\log T)^2+d(\log T)^3+e(\log T)^4+f(\log T)^5+g(\log T)^6+h(\log T)^7+i(\log T)^8}$$

to be used for describing the specific heat of aluminum or copper. The fitting coefficients are given in Table 2.

Coeff.	OFCH Copper	6061-T6 Aluminum
a	-1.91844	46.6467
b	-0.15973	-314.292
c	8.61013	866.662
d	-18.99640	-1298.30
e	21.96610	1162.27
f	-12.73280	-637.795
g	3.54322	210.351
h	-0.37970	-38.3094
i	0	2.96344
Data range	4-300 K	4-300 K

**Table 2.** Specific heat fitting coefficient.

The specific heat of copper and aluminum alloy has been calculated after [8] for the temperature interval of interest 77 – 300 K. It is graphically presented in Fig. 2 and some typical values are given in Table 3.

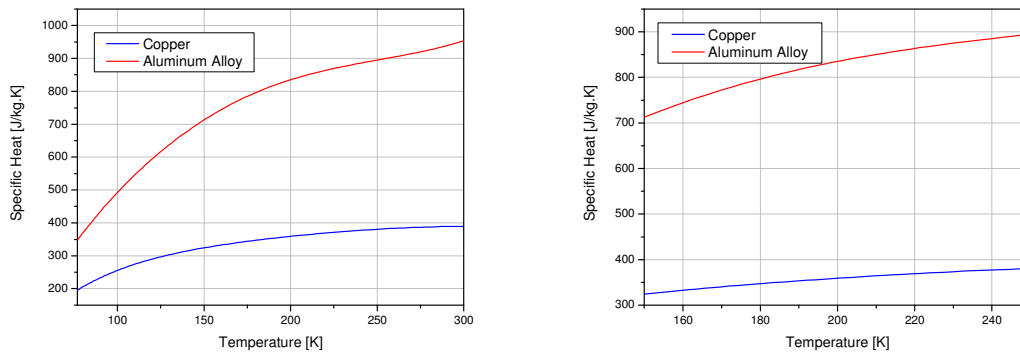


**Fig. 2.** Specific heat vs. temperature for copper and aluminum alloy.

Material	77 K [10 <sup>-3</sup> J/kg.K]	100 K [10 <sup>-3</sup> J/kg.K]	150K [10 <sup>-3</sup> J/kg.K]	200 K [10 <sup>-3</sup> J/kg.K]	300 K [10 <sup>-3</sup> J/kg.K]
<b>Cu</b>	0.196	0.255	0.324	0.359	0.389
<b>Al-6061-T6</b>	0.348	0.492	0.713	0.835	0.954

**Table 3.** Specific heat vs. temperature of technical materials (after [8]).

It is shown that calculated data for the aluminum alloy fully covered those given by Ekin [2], while in the copper case the deviation is less than 2 %.

### 1.3. Experimental Set-up.

Since the inner construction of the cooling engine X-Cooler II is not provided and the engine itself stays under the producer patent, only comparative test temperature measurements might be considered in order to evaluate its cooling power.

The cooling power test fixture is shown in Fig. 3 and the fixing to the cooling engine is given in Fig. 4. Two test elements have been designed: an aluminum alloy element with mass of 97 g and a copper element with mass of 414 g respectively. On the aluminum bar have been installed a Pt100 temperature sensor at 28 mm from the common surface and a heating element with 330 Ohm resistivity and 20 W power capability close to the open end of the bar. The copper element has a Pt100 temperature sensor installed at 66 mm from the common surface. The heating element was glued by DeltaBond thermal conducting compound. In order to minimize the uncontrolled temperature load through the contact surface the aluminum test element has been covered with Mylar known to be characterized with very low thermal emissivity.

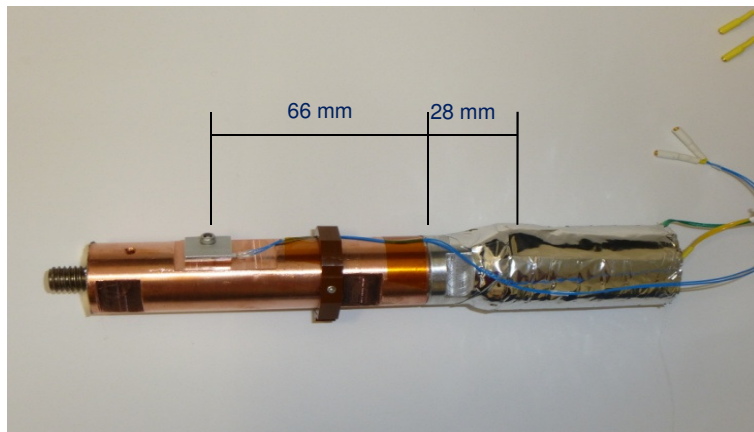


**Fig. 3.** Cooling power test fixture.

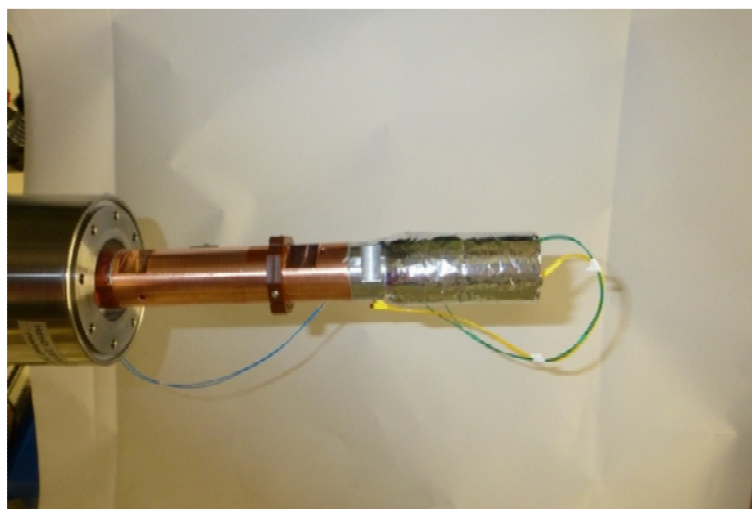


**Fig. 4.** Cooling test power fixture – cooling engine set-up. .

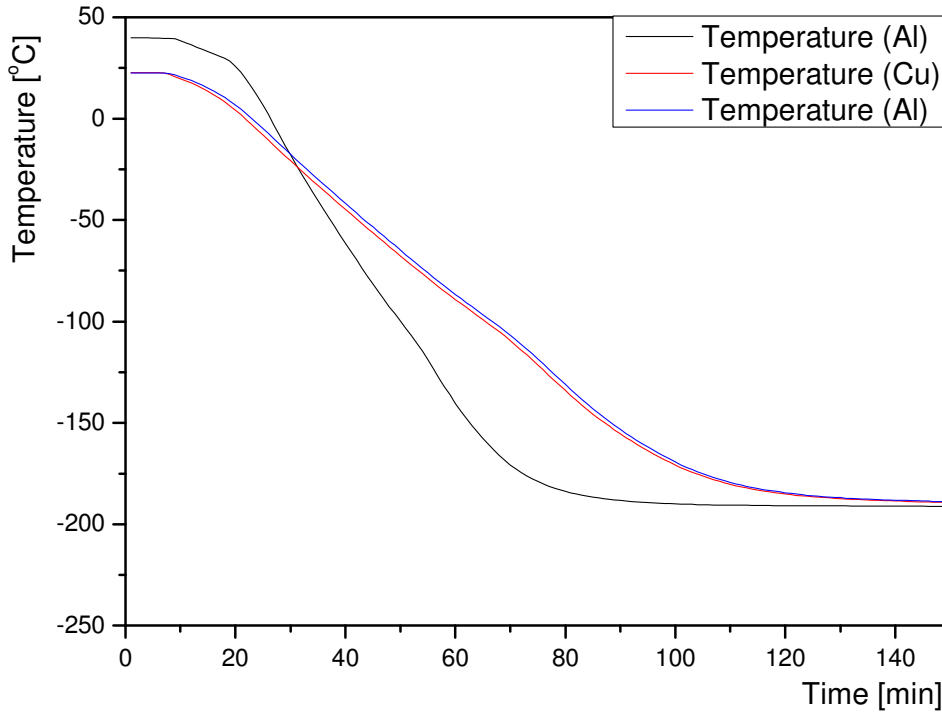


**Fig. 5.** Temperature development vs. time: black line (aluminum temperature, single element); red line (copper temperature, double element); blue line (aluminum temperature, double element).

At the first experiment only the aluminum test element was mounted and monitored. Then the both test elements were mounted as shown above and the cooling temperatures on both elements have been measured.

In terms of heat capacity the following equation are valid:

$$(12) \quad m_x \cdot \sum_{T_1}^{T_2} c_x (T_i - T_{i-1}) + m_{Al} \cdot \sum_{T_1}^{T_2} c_{Al} (T_i - T_{i-1}) = Q \cdot (t_2^s - t_1^s)$$

$$(13) \quad m_x \cdot \sum_{T_1}^{T_2} c_x (T_i - T_{i-1}) + m_{Al} \cdot \sum_{T_1}^{T_2} c_{Al} (T_i - T_{i-1}) + m_{Cu} \cdot \sum_{T_1}^{T_2} c_{Cu} \cdot (T_i - T_{i-1}) = Q \cdot (t_2^d - t_1^d).$$

and finally

$$(14) \quad m_{Cu} \cdot \sum_{T_1}^{T_2} c_{Cu} \cdot (T_i - T_{i-1}) = Q \cdot [(t_2^d - t_1^d) - (t_2^s - t_1^s)].$$

Here with  $t_i^s$  and  $t_i^d$  are denoted the time when the single element and the Al part of the two elements test fixture respectively reached the temperature  $T_i$  ( $i=1,2$ ) are denoted.

Initial Temperature T <sub>1</sub> [K]	Final Temperature T <sub>2</sub> [K]	Time single test element [min]	Time double test element [min]	Cooling power [W]
296	184	27	52	11.4
296	100	50	95	10.4
185	100	25	43	10.2

**Table 4.** Calculated cooling power.

In Table 4 is given the calculated cooling power. The estimate has been performed when different temperature intervals have been considered in order to approve that the evaluation is relatively independent on the temperature intervals contemplated.

## 2. Measurement of the temperature increase in dependence of the applied thermal load.

By cooling there is a strong correlation at low temperature between the thermal load applied and the resulting equilibrium temperature T within the test body. That is why the test system with a single test element has been investigated how it reacts when the external thermal load was applied. The measure data are graphically shown in Fig. 6.

Just 3 W applied results in 12 K increase in the equilibrium temperature. The factors affecting the temperature are the thermal contacts, the thermal losses due to radiative transfer, thermal bridges and residual gas heating and from another side are due to the thermal gradients along the test body.

Since the internal structure of the cooling head is unknown and the test fixture is relatively small and simple, the thermal losses can be neglected and to consider the equilibrium temperature as a function of only the thermal conductivity and the thermal contacts. Indeed, due to the good thermal conductivity of the cooper and the aluminum, the thermal contacts should be considered as the main factor determining the final temperature of the structure under cooling.

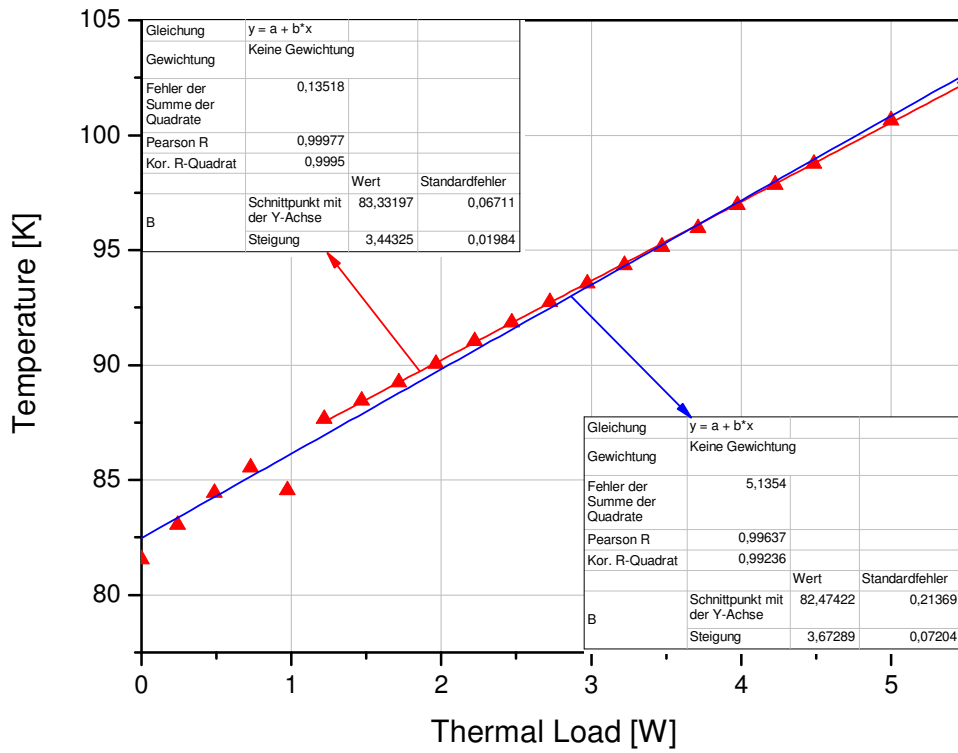


**Fig. 6.** Temperature increase vs. thermal load.

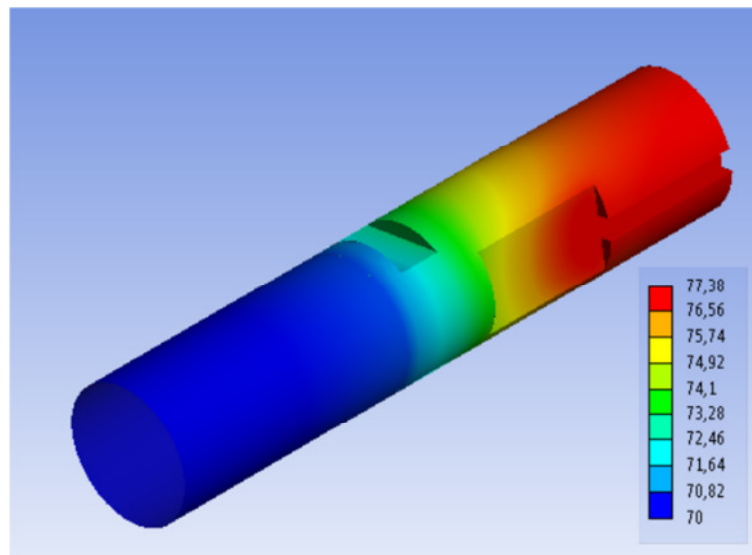


**Fig. 7.** Temperature distribution along the surface of Aluminum test element with an emissivity of 0.03, head emissivity of 0.25 and thermal load of 4 W.

### 3. Measurement of the thermal contact resistance

As it has been mentioned the thermal contact resistance is of paramount importance for the temperature deviations along the detector assembly.

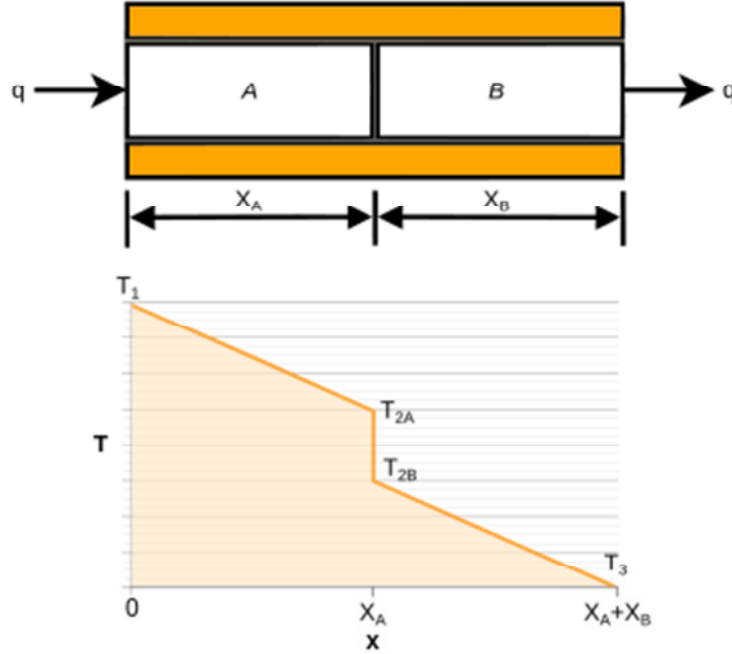


**Fig. 8.** Heat flow between two solid bodies in contact and the temperature distribution (reprinted from Wikipedia)

When two solid bodies are in contact a temperature drop is observed at the interface. This phenomenon is said to be a result of a thermal contact resistance existing between the contacting surfaces. Thermal contact resistance  $R_c$  is defined as the ratio between this temperature drop and the average heat flow across the interface

$$(15) \quad R_c = \frac{\Delta T}{Q} = \frac{\Delta T}{q \cdot A} = \frac{1}{h_c \cdot A} .$$

Here  $h_c$  is the thermal contact conductance coefficient,  $Q$  is the total flux,  $q$  is the heat flux density and  $A$  stays for the contacting area.

In practice the known temperatures are  $T_{Al}$  and  $T_{Cu}$  taken in distance  $\Delta x_{Al} = 28 \text{ mm}$  and respectively  $\Delta x_{Cu} = 66 \text{ mm}$  from the contact interface (s. Fig. 3). So that the conductance coefficient is to be defined due to the formulae:

$$(16) \quad \frac{T_{Al} - T_{Cu}}{q \cdot A} = \frac{1}{h_c \cdot A} + \frac{\Delta x_{Al}}{k_{Al} \cdot A} + \frac{\Delta x_{Cu}}{k_{Cu} \cdot A} .$$

Or

$$(17) \quad \frac{T_{Al} - T_{Cu}}{q} = \frac{1}{h_c} + \frac{\Delta x_{Al}}{k_{Al}} + \frac{\Delta x_{Cu}}{k_{Cu}} .$$

The contact area in the case under consideration is  $5.6 \cdot 10^{-4} \text{ m}^2$  and the both Al and Cu parts have been fixed by screwing with non-trouble force resulting in a momentum

os 20N.m. The whole assembly has been fixed to the X-Cooler cold finger with a momentum of 28 N.m. These values are just the limit of stability of the materials used.

The aluminum and copper are well conducting material. By the temperature of 85 K the thermal conductivity of aluminum alloy AW-5083 is equal to 59 W/m.K and of copper wit residual-resistivity ratio RR 50 is 480 W/m.K.

The scan of the measured temperature development for the first and the second run are shown in Fig. 7 a,b.

The measurements have been started when the forced thermal load is taken to be zero. Then the only active thermal load acting through contact area is those one determined by the radiative warming which is given also in Table 5.

Here the heat thermal emissivity has been considered to vary between 0.15 and 0.25 while the heat emissivity of the aluminum test element is taken to be within the range of 0.03 – 0.05. Because of the low surface area of the aluminum test element the estimate load is even below 0.12 W. That’s why even by a force thermal load of 3 W an accuracy of less than 5 % has been provided.

Head emissivity	Test element emissivity	Thermal Load [W]
0.15	0.05	0.12
0.15	0.03	0.075
0.25	0.03	0.08

**Table 5.** Thermal load in dependence on head and test element emissivity.

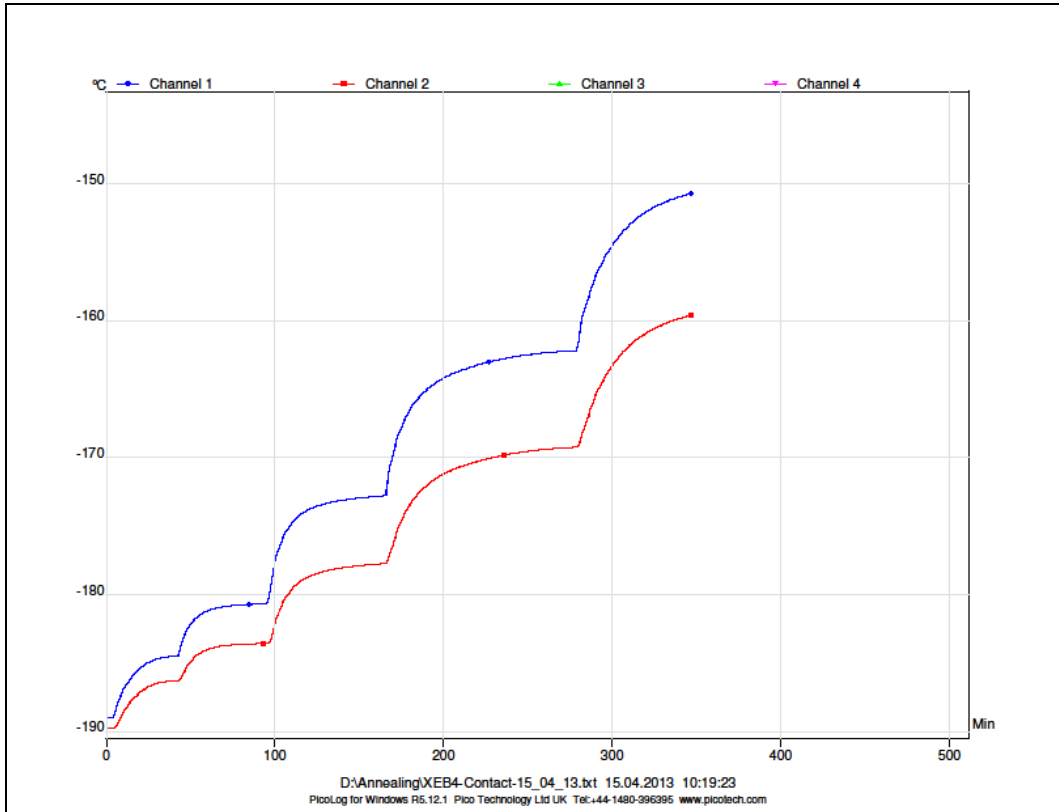


**Fig. 9 a.** Temperature development in dependence on the thermal load applied (first run).

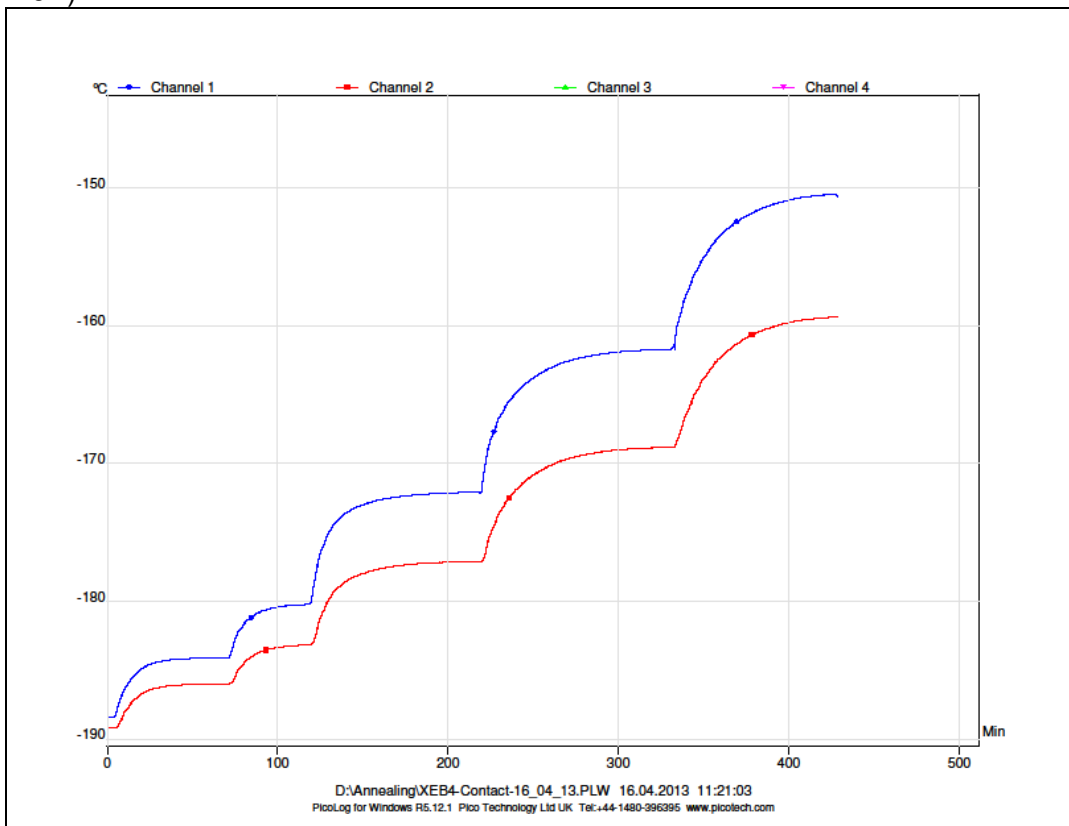


**Fig. 9 b.** Temperature development in dependence on the thermal load applied (second run).

The measured temperature-differences depend on the temperature load applied and are given in Table 5.

Thermal Power [W]	Temperature difference [K]
<b>First measurement</b>	
0.00	0.78
0.98	1.81
1.96	2.89
3.98	4.96
6.14	7.00
8.14	8.89
<b>Second measurement</b>	
0.00	0.81
0.98	1.88
1.98	2.95
3.99	5.02
6.13	7.10
8.13	8.69

**Table 6.** Measured temperature differences in dependence on the thermal load applied.

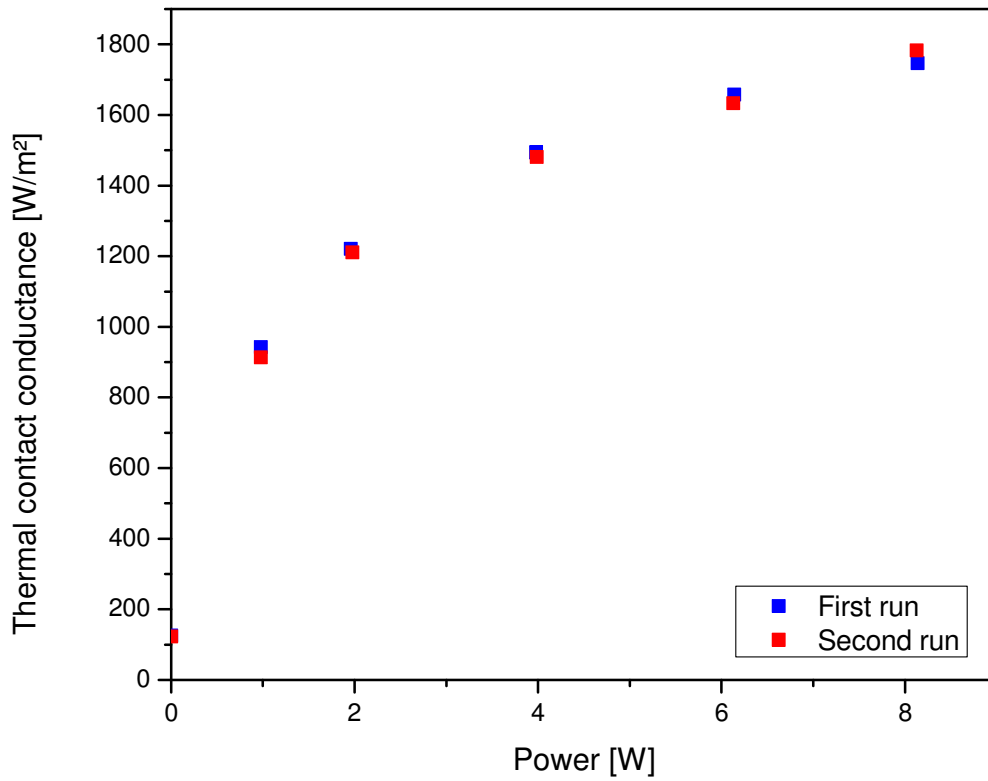


**Fig. 10.** Thermal contact resistance as a function on the thermal load applied.

Even by a heat load of 1 W the temperature deviation within the aluminum and the copper side of the test element is less than 1 K. To illustrate that the temperature distribution along the surface of Aluminum test element with an emissivity of 0.05, head emissivity of 0.15 and thermal load of 1 W is given in Fig. 9.

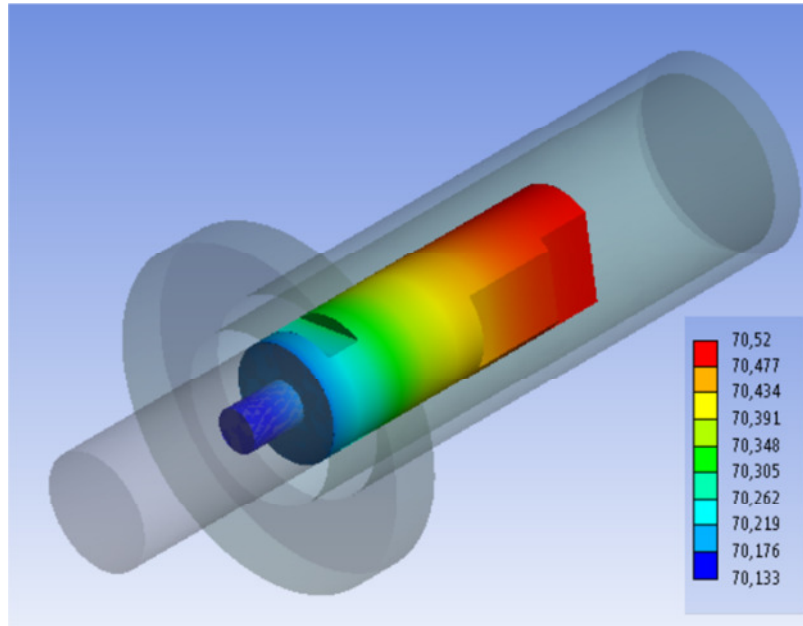


**Fig. 11.** Temperature distribution along the surface of Aluminum test element with an emissivity of 0.05, head emissivity of 0.15 and thermal load of 1 W.

Mylar is known to be a material with very low emissivity of 0.03. To minimize the radiative warming aluminum test element was fully covered with Mylar (s. Fig. 3). So that the heat losses due to the radiative warming of the aluminum part of the test element are less than 0.1 W (s. Table 5).

Head emissivity	Test element emissivity	Heat losses [W]	Heat flux density [ $\text{W}/\text{m}^2$ ]	Conductance coefficient [ $\text{W}/\text{m}^2 \cdot \text{K}$ ]
<b>0.15</b>	0.05	0.12	$2.1 \cdot 10^2$	1242
<b>0.15</b>	0.03	0.075	$1.3 \cdot 10^2$	604
<b>0.25</b>	0.03	0.08	$1.4 \cdot 10^2$	660

**Table. 7.** Thermal contact conductance coefficient.

Finally the thermal contact conductance coefficient is determined and given in Table 6. As it has been already shown (Report from September) even thermal conductance of  $1000 \text{ W}/\text{m}^2 \cdot \text{K}$  is to give increase of germanium crystal with 4 K. A conclusion should be drawn that special attention with respect to the construction of the thermal contact is to be drawn.

In general the thermal contact resistance is a strong dependent function on thermal conductivity of the contacting materials, pressure between the contacting materials, geometry of the contacting surface etc.

With the temperature decrease the thermal conductance decrease also and becomes very low at cryogenic temperature (s. Fig. 7, reprinted from [2]). Fig. 10 summarizes the results for solder, varnish, and grease joint. However, the curves for the pressure joint give the total conductance of the joint, independent of the contact area, but

dependent on the total force applied. Dashed lines are estimates of the conductance in temperature regions where no data are available.

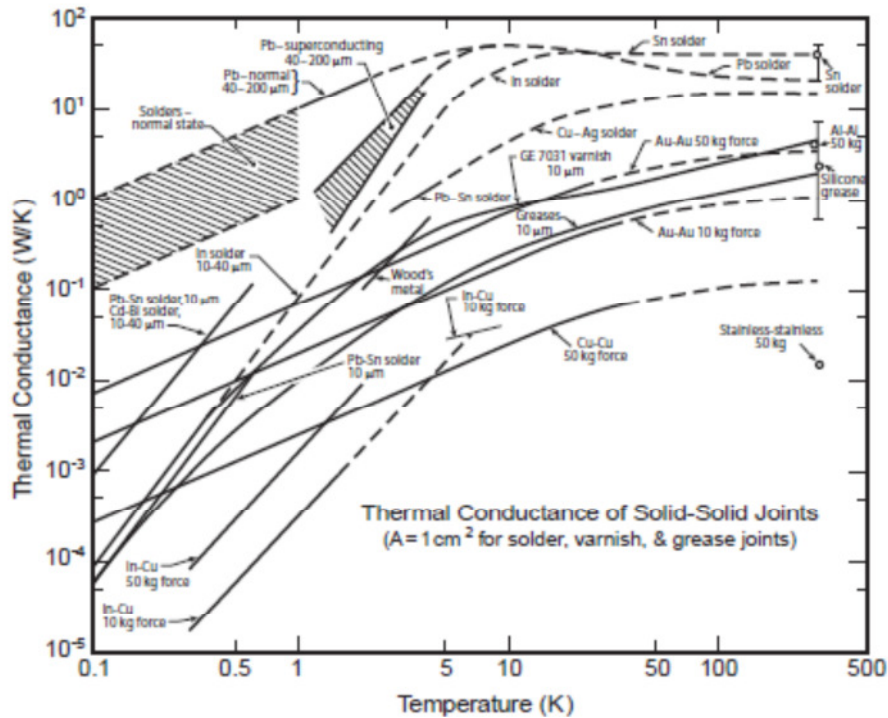


**Fig. 12.** Thermal conductance as a function of temperature for solder, varnish, grease.

Heat conduction across solid interface pressed together with 445 N Force also is given by Ekin [2] and reproduced again here

Interface materials	4.2 K	77 K
Copper/copper	$1 \times 10^{-2}$ W/K	$3 \times 10^{-1}$ W/K
Steel/steel	$5 \times 10^{-3}$ W/K	$3 \times 10^{-1}$ W/K

**Table 8.** Thermal conductance across solid interface of 1 cm<sup>2</sup> pressed with 445 N.

**4. Examination of the labyrinths geometry in respect of the heat losses.**

In order to verify the fixing labyrinth geometry the labyrinth with five, four and three ring respectively has been examined. The labyrinth material has been supposed to be polyethylene with the thermal conductivity of 0.28 W/m.K.

The structural steel sleeve is to be used to get together the labyrinth with the cold finger. A typical thermal conductivity of the structural steel is 60.5 W/m.K.

The three scenarios mentioned have been simulated and the results obtained are presented in the figures below.

In Fig. 13-15 the temperature distribution along the surface of the polyethylene fixing labyrinth and the structural steel sleeve is shown. The temperature of the warm part is considered to be 295.15 K and of the cold finger 70 K.

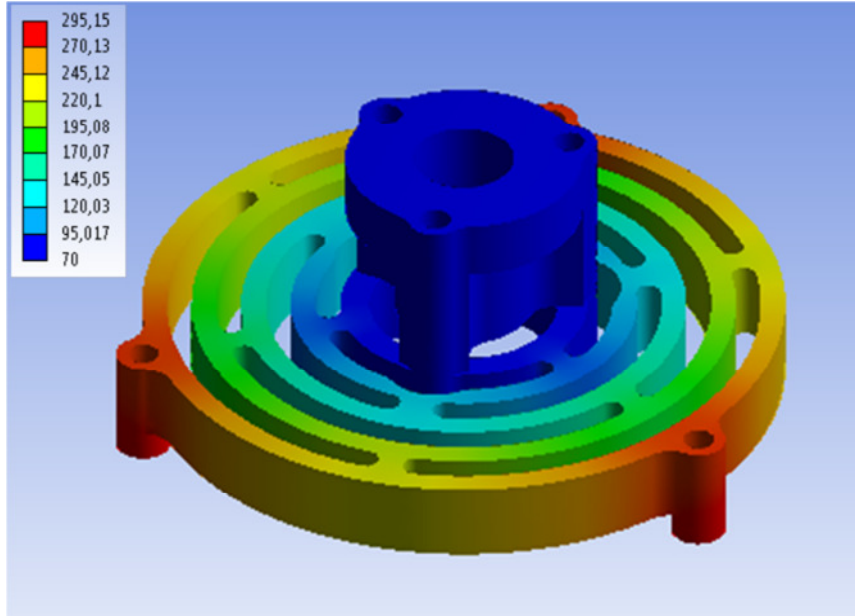


**Fig. 13.** Temperature distribution along the surface of the polyethylene five rings fixing labyrinth and the structural steel sleeve.

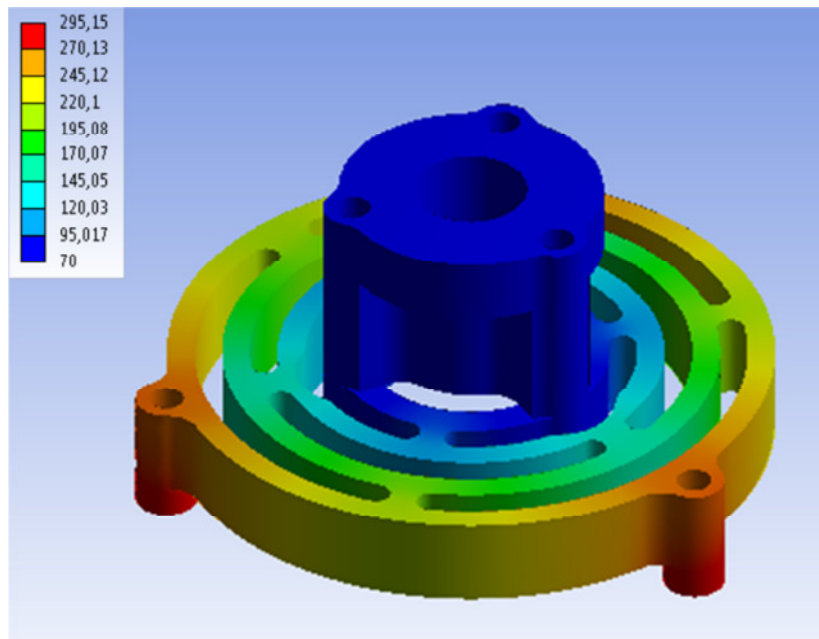


**Fig. 14.** Temperature distribution along the surface of the polyethylene four rings fixing labyrinth and the structural steel sleeve.

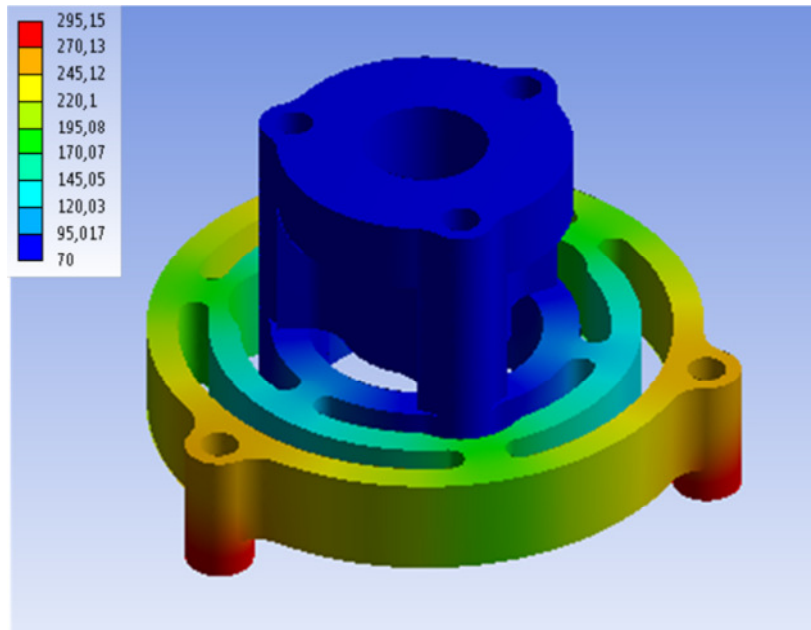


**Fig. 15.** Temperature distribution along the surface of the polyethylene three rings fixing labyrinth and the structural steel sleeve.

The resulted heat losses are summarized in Table

Labyrinth design	Heat losses [W]
<b>5 rings</b>	0.056
<b>4 rings</b>	0.077
<b>3 rings</b>	0.112

**Table 9.** Heat losses in dependence on the geometric labyrinth arangement.

By the basic labyrinth geometry with five rings the heat losses are evaluated to be 0.056 W. When remove one of the rings the heat losses are to increase with 37.5 % that are to reach 0.077 W. If one more ring is to be removed the heat losses are to increased twice and are evaluated to be 0.112 W.

As a cost saving solution four rings design is proposed. Hire is also to mention that the bed-plate could be shortened without to worse the heat performance.

### Reference

1. W. Polifke, J. Kopitz, Wärmeübertragung. Grundlagen, analytische und numerische Methoden, Pearson Studium, 2005.
2. J. W. Ekin, Experimental techniques for low temperature measurements, Oxford University Press, Oxford 2006.
3. Corruccini, R.J., and Gniewek, J.J. (1961), Thermal Expansion of Technical Solids at Low Temperatures. NBS Monograph 20, pp. 1-20. US Government Printing Office, Washington, DC.
4. Chang, S.S. (1977). "Heat capacity and thermodynamic of polyvinyl chloride", J. Res. Natl. Bur. Stand. 82, 9-17.

5. Touloukian, Y.S. (1966). Recommended Values of the Thermodynamical Properties of Eighth Alloys Major Constituents and their Oxides, Report No. CST-7590, 271-343, Thermodynamical Properties Research Center, Purdue University, Lafayette, IN.
6. Johnson, V. (1960). A Compendium of the Properties of Materials at Low Temperature, Part II, Properties of Solids, WADD Technical Report 60-56. National Bureau of Standards and Wright Air Development Division, US Government Printing Office, Washington DC.
7. White, G.K. and Meeson, P.J. (2002). Experimental Techniques in Low-Temperature Physics, 4<sup>th</sup> Edition, Oxford, UK.
8. E.D. Marquardt, J.P. Le, and Ray Radebaugh, Cryogenic Material Properties Database, National Institute of Standards and Technology, Boulder, CO 80303.